PROCEEDINGS, 51st Workshop on Geothermal Reservoir Engineering
Stanford University, Stanford, California, February 9-11, 2026
SGP-TR-230

Integrated Seismic Monitoring during 2025 Reservoir Stimulations at the Newberry EGS field, Oregon

Nori Nakata[1], Chet Hopp[1], Parker Sprinkle[2], Michael E. Mann[2], Zhengfa Bi[1], Jinxiao Liu[1], Alain Bonneville[3], Gabrijel Grubac[3], Natalia Mychaluk[4], Laura N. Torres[4]

[1]Lawrence Berkeley National Laboratory, [2]Pacific Northwest National Laboratory, [3]Mazama Energy, [4]Halliburton

nnakata@lbl.gov

Keywords: EGS, seismic monitoring, Newberry, DAS

ABSTRACT

We present the recent effort of the seismic monitoring system at the Newberry Enhanced Geothermal System (EGS) site. The network comprises eight borehole sensors reaching depths of up to 300 m—six legacy 2 Hz geophones (NN07, NN09, NN17, NN19, NN21, NN24) that have been continuously operational since 2012, and two broadband accelerometers (NN18 and NN32) added in 2023 to extend the frequency bandwidth and dynamic range. Data from all sensors is streamed in near real time to the EarthScope Data Management Center (DMC), where it is publicly accessible.

Additional regional coverage is provided by nearby stations operated by the University of Washington's Pacific Northwest Seismic Network (PNSN) and the USGS Cascades Volcano Observatory (CVO). All seismic data are processed in real time using LBNL's automated detection and analysis pipeline, which identifies, locates, and estimates magnitudes of induced events associated with injection activities at the Newberry site.

To enhance spatial and temporal resolution during reservoir stimulation, we also deploy borehole distributed acoustic sensing (DAS) and a surface nodal network consisting of 90 nodes. Microseismic Inc. was contracted to deploy a dense array of nodal sensors to better detect seismicity in real-time during stimulations in 55A-29 in July 2025. We analyze seismic signals from two 2025 stimulations (January and August) and compare them with the 2012 and 2014 experiments. Although the 2025 campaigns generated fewer detectable seismic events, the DAS captures coherent P and S wave propagation, which are useful to locate the events. Because the surface stations do not record clear wavefields due to their signal-to-noise ratio, the earthquake size is expected to be much smaller than 2012 and 2014 stimulations.

1. INTRODUCTION

The Newberry Volcano EGS project implemented a first-of-its-kind propped hydraulic stimulation in an extreme super-hot rock environment (>300 °C) to enhance permeability in a dry, crystalline reservoir. The stimulation focused on the recompleted NWG 55-29 injector well and its adjacent producer (55A-29), using a carefully designed multistage approach that combined high-pressure injection, thermally stable proppants, hybrid stimulation fluids, and innovative completion technologies, including the world's first stimulation sleeve rated above 300 °C. Real-time diagnostics—such as distributed temperature and acoustic sensing (DTS/DAS), microseismic monitoring, nanoparticle tracers, and acoustic friction analysis—were used to constrain fracture geometry, connectivity, and fluid distribution. Despite injection pressures comparable to earlier campaigns, the 2025 stimulation induced remarkably low seismicity, consistent with prior stress interpretations and indicating reduced seismic risk. These initial results demonstrate the successful creation of propped fracture networks with enhanced flow potential and validate Newberry as a leading testbed for scalable super-hot EGS development (Grubac et al., 2025).

Seismic monitoring is a fundamental component of enhanced geothermal system (EGS) development. Induced seismicity provides the most direct observational window into fracture activation, stress redistribution, and fluid migration during stimulation and subsequent circulation (Atkinson et al., 2020). In a volcanic setting such as Newberry, characterized by elevated temperatures and complex stress conditions, continuous seismic observations are essential for tracking the spatiotemporal evolution of seismicity relative to injection operations. Such monitoring is crucial for seismic risk mitigation strategies, including traffic-light–based operational controls, by enabling rapid assessment of event rates, magnitudes, and spatial migration that may signal increased hazard.

Beyond seismic hazard management, detailed monitoring of microseismicity plays a critical role in reservoir characterization and stimulation optimization. Dense seismic observations lower the magnitude of completeness, allowing detection of small-magnitude events that illuminate fracture geometry, connectivity, and reservoir growth well before larger events occur. These observations provide key constraints on subsurface stress orientations, active fault structures, and permeability pathways, informing thermo-hydro-mechanical interpretations and guiding adaptive stimulation strategies (Nakata et al., 2025). We can also reveal subsurface structure with continuous seismic recordings and micro earthquakes (Brenguier et al., 2016; Nakata and Shelly, 2018). As EGS projects at Newberry advance toward higher temperatures and more ambitious stimulation goals, robust seismic monitoring remains essential not only for safe operations but also for improving reservoir performance and advancing understanding of fracture processes in volcanic geothermal systems.

Here, we present the seismic monitoring system deployed at the Newberry EGS field, including both permanent and temporary instrumentation, and summarize initial observations from the 2025 stimulation campaign.

2. DATA ACQUISITION

The backbone seismic monitoring system currently deployed at the Mazama Newberry EGS site closely resembles the configuration used during AltaRock's earlier projects in 2012 and 2014 (Sonnenthal et al., 2015; Cladouhos et al., 2016). It includes eight sensors placed in boreholes reaching depths of up to 300 meters (Figure 1a). Of these, six (NN07, NN09, NN17, NN19, NN21, and NN24) are the original 2 Hz geophones since 2012, while the remaining two (NN18 and NN32) are broadband accelerometers added in 2023. The collected data is streamed nearly in real time to the EarthScope Data Management Center (DMC), where it is publicly accessible. Additional seismic coverage is provided by nearby stations operated by the University of Washington's Pacific Northwest Seismic Network (PNSN) and the USGS Cascades Volcano Observatory (CVO). All data from these stations is processed in real time using LBNL's detection and analysis system, which identifies, locates, and estimates magnitudes of seismic events related to the ongoing injection activities at the Newberry site. We detected only a few events during January and July 2025 stimulations with the backbone seismometers (Figure 2).

In addition to the backbone seismic network, we deployed a temporal nodal array with SmartSolo three-component 5Hz IGU sensors (Figure 1b). The sensor has a battery for continuous recording of 25-30 days. Similar to Nakata et al. (2025), each location has two sensors, and one has a delayed start to continuously record seismic activities over 50 days without maintenance. 10 stations have an external battery, which allows us to record 4 months of data. We deployed a total of 90 nodes at 50 locations.

A distributed acoustic sensing (DAS) fiber was also installed in well 55-29 (Figure 3) for seismic monitoring and to improve understanding of reservoir stimulation via fracture characterization and imaging. DAS recordings were acquired in the 55-29 well during two stimulations in January and July 2025. Despite being much closer to the stimulation than the surface sensors and being more sensitive, only 38 events were detected and located by Halliburton using the downhole DAS array during stimulation of 55-29.

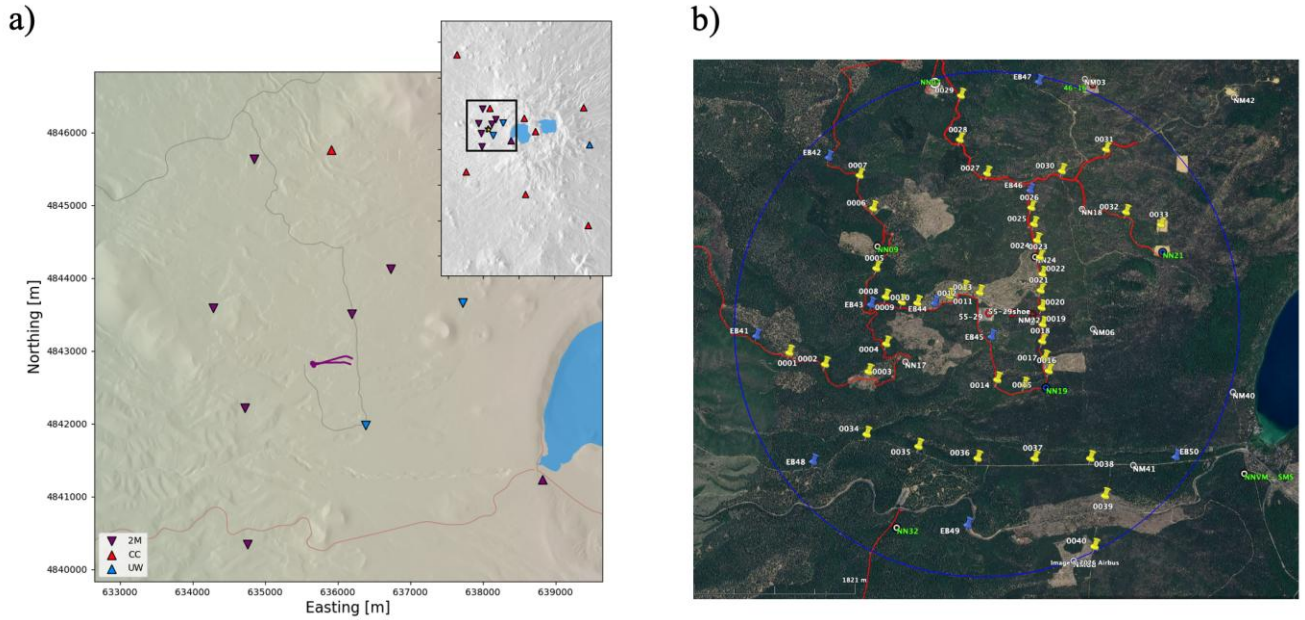

Figure 1. (a) Map of the seismic monitoring network at the Mazama EGS site. The injection well (55-29) is shown as a purple stem with a circle at the wellhead. Purple inverted triangles indicate the locations of stations with telemetry is hosted by LBNL, blue triangles indicate telemetry hosted by PNSN, and red triangles are operated by USGS (CVO). A strong-motion sensor is installed in a forest service warehouse to the southeast (black triangle). (b) Map of the temporary nodal stations deployed by LBNL (yellow and blue pins). 90 nodes are deployed along roads (red and gray lines) at 50 locations. The blue pins indicate nodes with external batteries for 4 months of continuous recording. The blue circle shows 3 km from Pad 29.

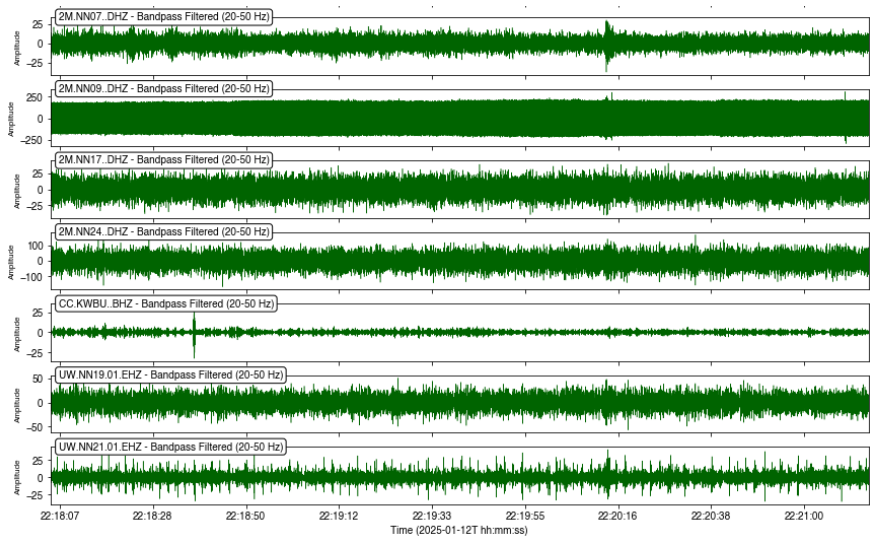

Figure 2. An example record of backbone seismometers for a ~M-0.9 earthquake around 22:20:12. We applied a bandpass filter of 20-50 Hz.

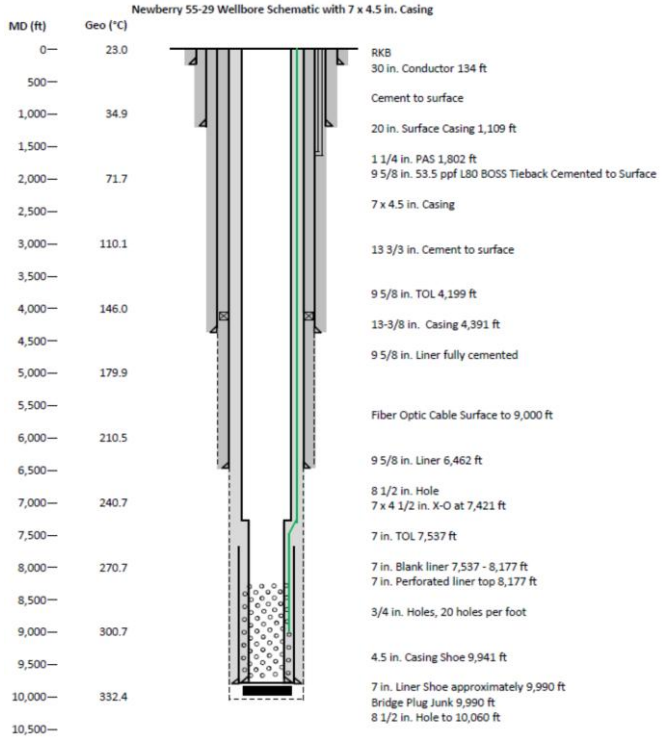

Figure 3. A schematic diagram of Well 55-29 with an installed fiber cable (green line). The fiber is located from the ground surface to around 9000 feet in depth and used for DTS/DAS acquisition.

3. DAS DATA PROCESSING

We reprocess the DAS data to refine the detection and location of the events. The data preprocessing workflow is designed to bridge the gap between a coarse existing seismic catalog and high-resolution event detection using DAS data. Because the available seismic catalog provides only approximate event origin times, a hybrid strategy combining manual picking, supervised machine learning, and classical signal processing is adopted.

3.1 Initial event time estimation from an existing seismic catalog

We start from the existing seismic catalog compiled from regional seismic stations. This catalog provides approximate event origin times associated with injection activities but lacks precise timing and completeness, especially for small-magnitude events. These cataloged times are therefore treated only as coarse temporal guides rather than exact detections. For each cataloged event, we extract a one-hour DAS data window centered on the reported origin time. This window is sufficiently long to accommodate uncertainties in the catalog timing while ensuring that the associated DAS wavefield is included.

3.2 Manual picking and construction of training data

Within each one-hour DAS window, all visually identifiable seismic events are manually picked. Manual picking is performed directly on DAS time–channel images, focusing on coherent P- and S-wave moveouts that are distinguishable from background noise. This step refines the approximate event times provided by the seismic catalog, and produces a high-quality labeled dataset for supervised learning.

Each manually identified event is converted into a labeled DAS image patch, containing both signal and representative noise examples. These labeled patches collectively form the training dataset for deep-learning-based detection.

3.3 ML-based detection of DAS image patches

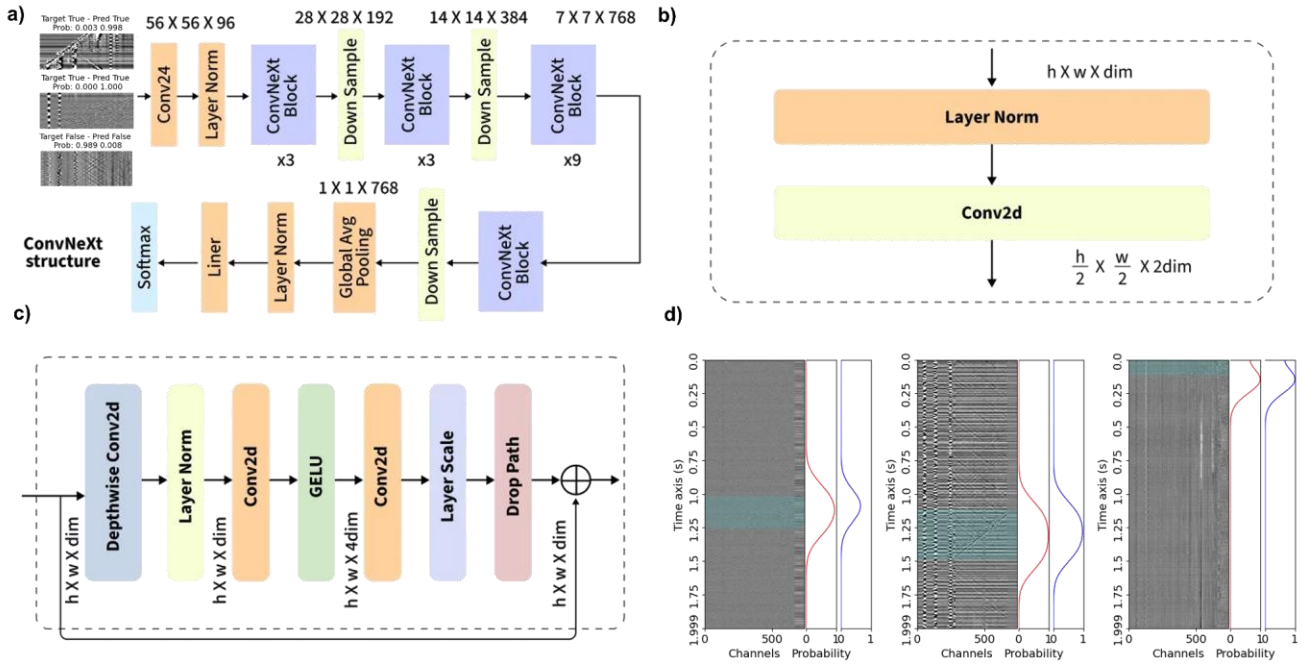

Figure 4: ConvNeXt architecture and model outputs. (a) Overall ConvNeXt network structure with hierarchical feature extraction and classification head. (b) Downsampling module composed of layer normalization and convolution. (c) ConvNeXt block design with depthwise convolution, pointwise transformations, and residual connection. (d) Example inputs and corresponding predicted class probabilities.

Using the manually labeled DAS image patches, we train a ConvNeXt–based convolutional neural network to automatically detect seismic events in DAS data. The ConvNeXt architecture is chosen for its ability to capture both local waveform features and larger-scale spatiotemporal coherence in DAS images.

The network is trained to perform pixel-level classification, distinguishing seismic signal regions from background noise. Once trained, the model is applied to continuous DAS data to identify candidate seismic event patches with high sensitivity, including events below the detection threshold of conventional surface stations. Figure 1 shows the ConvNeXt-based architecture and example model outputs used in this study. The overall network structure, including the hierarchical feature extraction stages and classification head, is shown in Figure 4a. The downsampling operation between stages, consisting of layer normalization followed by convolution, is detailed in Figure 4b, while the internal design of an individual ConvNeXt block with depthwise convolution, pointwise transformations, and residual connection is displayed in Figure 4c. Example input DAS image patches and the corresponding predicted class probabilities are shown in Figure 4d.

Using the manually labeled DAS image patches, we train a convolutional neural network to automatically detect seismic events in DAS data. The network is designed to capture both local waveform characteristics and larger-scale spatiotemporal coherence in DAS images (Figure 4a–c). It is trained to perform pixel-level classification, distinguishing seismic signal regions from background noise. Once trained,

the model is applied to continuous DAS data to identify candidate seismic event patches with high sensitivity, including events below the detection threshold of conventional surface stations, as illustrated by the prediction examples in Figure 4d.

After the detection scheme, we detect nearly three times as many earthquakes as shown in the catalog. Note that these numbers are still smaller than the earthquakes recorded during the 2014 stimulation and also much smaller magnitudes.

3.4 Denoising workflow

For each candidate event detected by the ConvNeXt model, we extract a shorter DAS window around the event moveout and apply a consistent denoising workflow prior to phase picking. The goal is to reduce instrumentation and environmental noise while preserving coherent moveouts in the well. The processing sequence is as follows.

1. **Detrending.** Each DAS channel is linearly detrended in time to remove slow drift and offsets.
2. **Common-noise removal (common-mode).** Spatially coherent noise is suppressed by subtracting a robust estimate of the common mode at each time sample, computed as the median across channels. This step reduces array-wide disturbances (e.g., interrogator-related or other spatially uniform components) while preserving coherent seismic moveouts.
3. **High-pass filtering.** The data are high-pass filtered with a 1 Hz frequency to attenuate long-period trends and very low-frequency noise.
4. **FK (frequency–wavenumber) filtering.** Finally, we apply FK-domain filtering to isolate coherent energy based on apparent velocity. Typical moveout speeds in our well DAS data are ~5900 m/s for P waves, ~3400 m/s for S waves, and ~1800 m/s for tube waves, so we choose a broad apparent-velocity passband that preserves these phases while suppressing near-zero-velocity components and incoherent energy. Specifically, we retain apparent velocities in two symmetric bands: −8000 to −1000 m/s and +1000 to +8000 m/s. This mask removes low-apparent-velocity energy that is commonly dominated by coherent noise and non-propagating artifacts, while keeping both upgoing and downgoing/reflecting wavefields within the physically expected velocity range.

Figures 5 and 6 illustrate the effect of the FK step on representative event windows. In Figure 5, the raw time–channel panel contains clear P and S moveouts from the well bottom as well as an oppositely propagating tube-wave branch. After FK filtering, both propagation directions are preserved within the selected velocity bands, but incoherent and low-velocity energy is reduced, sharpening the moveouts and improving phase readability. In Figure 6, the raw window is dominated by a strong tube wave and a secondary branch interpreted as a reflected tube wave generated by boundary-condition changes along the well. After denoising and FK filtering, the tube-wave moveouts are cleaner and a weaker P-wave arrival becomes more apparent in the processed window.

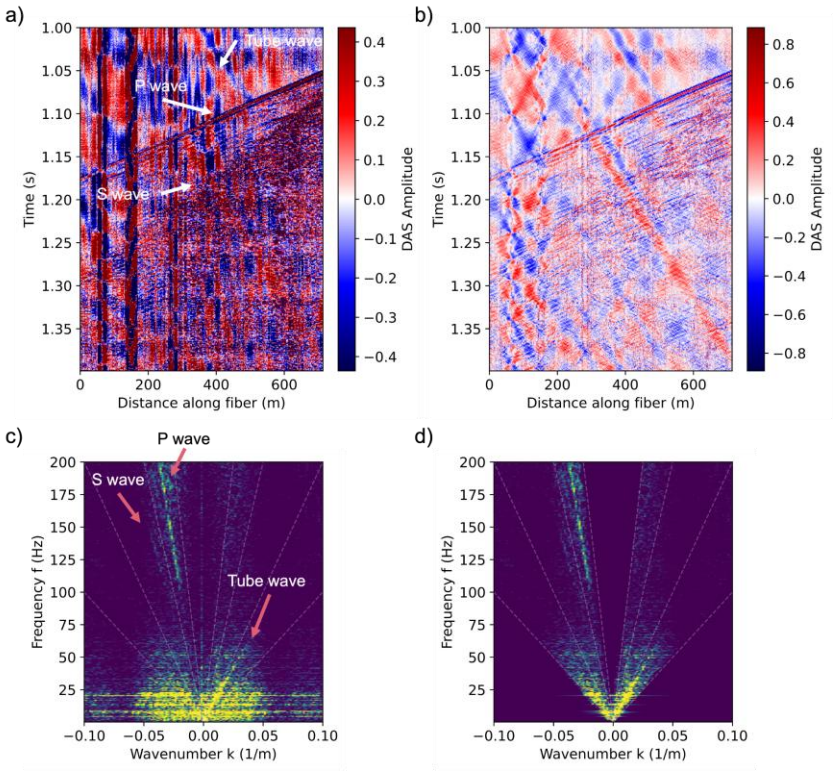

Figure 5: Example of P/S waves in a detected DAS window. (a) Raw DAS time–distance image. (b) The same window after the denoising workflow, where coherent moveouts are sharpened and low-apparent-velocity/incoherent energy is reduced. (c) FK amplitude spectrum of (a); dotted lines indicate constant apparent velocities of −1000, −2000, −4000, −8000, +8000,

+4000, +2000, and +1000 m/s. (d) FK spectrum after applying the velocity mask, retaining energy within −8000 to −1000 m/s and +1000 to +8000 m/s.

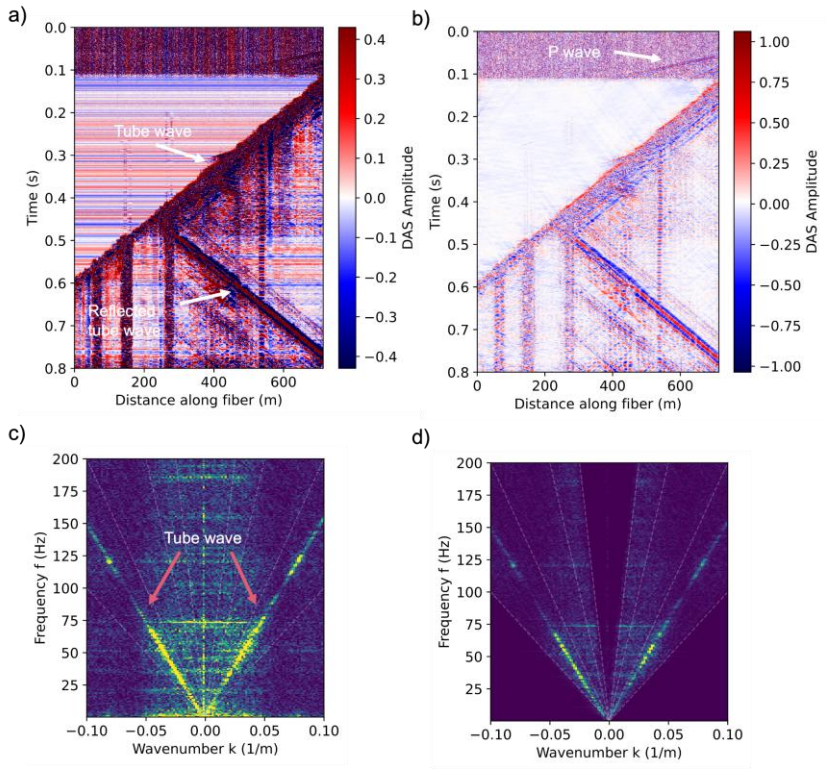

Figure 6: Example of tube waves in a detected DAS window. (a) Raw DAS time–distance image. (b) The same window after the denoising workflow. (c) FK amplitude spectrum of (a). (d) FK spectrum after applying the velocity mask, retaining energy within −8000 to −1000 m/s and +1000 to +8000 m/s.

3.5 Precise event time determination and phase picking using STA/LTA

The ConvNeXt detector outputs candidate DAS image patches that contain seismic signals but do not directly provide precise arrival times. We therefore refine event timing and extract phase information after the denoised windows described in Section 3.4. For each detected patch, we compute a short-term average to long-term average (STA/LTA) characteristic function on a subset of DAS channels that exhibit strong inter-channel coherence after denoising, and we take the time of the maximum STA/LTA ratio as the refined event onset time. Using the same processed event window, we then pick P- and S-wave arrivals on DAS time–distance images. Picks are made over a channel interval with strong coherence and are validated by tracking the onset across neighboring channels to ensure consistency of the moveout trend. Figure 7 shows a representative denoised event window in which coherent P and S moveouts are clearly resolved, enabling robust phase identification and picking relative to the STA/LTA-derived onset time.

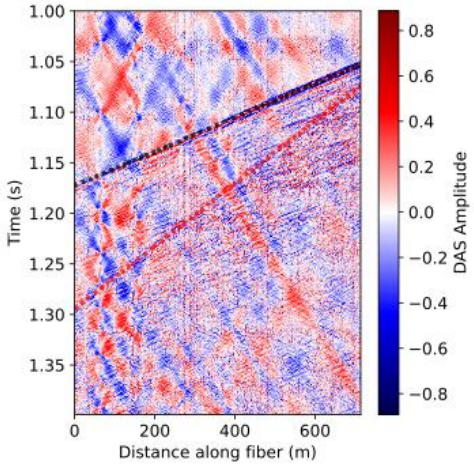

Figure 7: Example of P- and S-wave picking in a denoised DAS event window, with the P- and S-wave moveouts highlighted by black and red pick lines, respectively.

3.6 Relocation of 38 events

To improve the accuracy of the earthquake locations, we reprocess the DAS waveforms for the 38 cataloged events with careful phase picking and relocation (Figure 8). Because the earthquakes are too small and no clear waves are observed at the surface, we use only DAS data for relocation. Because of the nature of DAS as a one-dimensional array, we have a non-uniqueness problem, or smearing effects, to locate the events. The DAS array in 55-29 is not completely linear, which is helpful to locate the events.

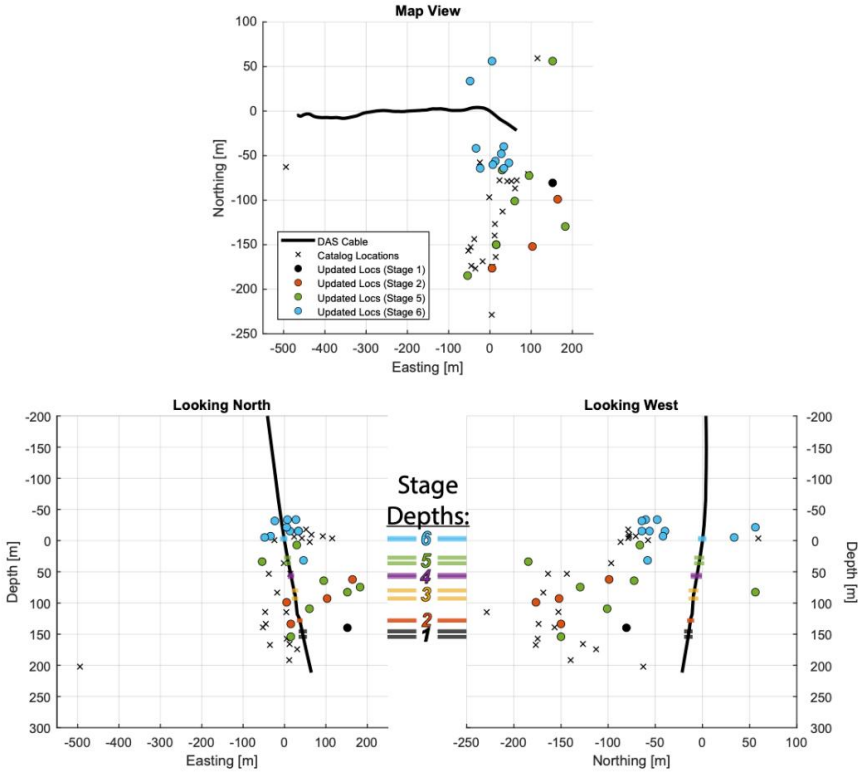

Figure 8: Revised hypocenters of the seismicity detected by DAS during stimulation of 55-29. X's indicate the locations from the onsite contractor. Filled circles show the revised locations, colored to match the stage of injection during which they occurred.

4. DISCUSSION AND CONCLUSIONS

The 2025 stimulation campaigns at the Newberry EGS site provide a valuable case study demonstrating both the opportunities and challenges of seismic monitoring in low-seismicity, super-hot geothermal environments. Despite injection pressures comparable to earlier campaigns, the induced seismicity during the 2025 operations was markedly limited, with only a small number of events detectable by conventional surface and shallow-borehole seismometers. This highlights a key monitoring challenge for modern EGS projects: as stimulation strategies evolve to minimize seismic hazard, the resulting seismic signals increasingly fall below the detection thresholds of traditional monitoring networks. In this context, downhole and near-field sensing, particularly distributed acoustic sensing (DAS), can potentially play a critical role by capturing coherent P- and S-wave propagation that would otherwise remain unobserved. The ability of DAS to resolve small-magnitude events near the stimulation interval underscores its value for characterizing fracture activation and stress response even when overall seismicity rates are low.

From a seismic monitoring perspective, the Newberry results emphasize the importance of integrated, multi-sensor networks that combine permanent instrumentation with targeted temporary deployments. Permanent borehole sensors provide long-term continuity and baseline characterization, while temporary nodal arrays and downhole DAS significantly enhance spatial resolution during active stimulation. Together, these systems enable robust detection, relocation, and interpretation of induced seismicity across a wide range of magnitudes and distances from the injection zone. As EGS development at Newberry advances toward higher temperatures and more complex stimulation strategies, such integrated monitoring frameworks will be essential not only for seismic risk management, but also for extracting meaningful reservoir information from sparse seismicity. More broadly, the Newberry experience illustrates that future EGS projects will increasingly rely on advanced seismic monitoring technologies and data-driven analysis methods to balance seismic safety with effective reservoir stimulation in challenging geological settings.

5. ACKNOWLEDGMENT

We would like to thank Mazama Energy management for their support and allowing the sharing of this case study. The LBNL part of this work was supported by the U.S. Department of Energy, Hydrocarbons and Geothermal Energy Office, under Award Number DE-AC02-05CH11231.

REFERENCES

Atkinson, G.M., Eaton, D.W. & Igonin, N. Developments in understanding seismicity triggered by hydraulic fracturing. Nat Rev Earth Environ 1, 264–277 (2020)

Brenguier, F., D. Rivet, A. Obermann, N. Nakata, P. Boué, T. Lecocq, M. Campillo, and N. Shapiro (2016), 4-D noise-based seismology at volcanoes: Ongoing efforts and perspectives, J. Volcanol. Geoth. Res., 321, 182-195, doi:10.1016/j.jvolgeores.2016.04.036

Cladouhos, T. T., S. Petty, M. W. Swyer, M. E. Uddenberg, K. Grasso and Y. Nordin (2016) Results from Newberry Volcano EGS Demonstration, 2010-2014, Geothermics, 63, 44-61.

Grubac, G., G. Gullickson, A. Bonneville, P. Brand, D. Goloshchapova, E.M. Dunham, M. Khan, T. A. Shokanov, D. Cuthill, C. Gibson, T. Palisch, C. Hopp and N. Nakata (2025) EGS Propped Stimulation >300°C: From Design to Implementation Phase I, SPE Annual Technical Conference and Exhibition, SPE-228078-MS.

Nakata, N., H. Chang, S.-M. Wu, Z. Bi, L.-W. Chen, F. Soom, H. Gao, A. Titov, and S. Dadi (2025) Fracture Characterization and Stress Communication Revealed by Induced Seismicity at the Cape Modern Geothermal Field, Utah, GRC Transactions, 49, 2025, 1191-1202.

Nakata, N. and D. R. Shelly (2018) Imaging a crustal low-velocity layer using reflected seismic waves from the 2014 earthquake swarm at Long Valley Caldera, California: The magmatic system roof?, Geophys. Res. Lett., 45, 3481-3488.

Sonnenthal, E. L., J. T. Smith, T. Cladouhos, J. Kim and L. Yang (2015) Thermal-hydrological-mechanical-chemical modeling of the 2014 EGS stimulation experiment at Newberry volcano, Oregon, Proceedings of Geothermal Reservoir Enginnering, SGP-TR-204.